BIOCHEMISTRY
including biophysical chemistry & molecular biology

Article

pubs.acs.org/biochemistry

Kinetic and Structural Basis for Acyl-Group Selectivity and NAD$^+$ Dependence in Sirtuin-Catalyzed Deacylation

Jessica L. Feldman,[†] Kristin E. Dittenhafer-Reed,[†,@] Norio Kudo,[§] Julie N. Thelen,[‡] Akihiro Ito,[∥] Minoru Yoshida,*[,§,∥,⊥] and John M. Denu*[,†,‡]

[†]Department of Biomolecular Chemistry and [‡]Wisconsin Institute for Discovery, University of Wisconsin—Madison, Madison, Wisconsin 53715, United States

[§]Seed Compounds Exploratory Unit for Drug Discovery Platform and [∥]Chemical Genomics Research Group, RIKEN Center for Sustainable Resource Science, Hirosawa 2-1, Wako, Saitama 351-0198, Japan

[⊥]CREST Research Project, JST, 4-1-8 Honcho, Kawaguchi, Saitama 332-0012, Japan

Supporting Information

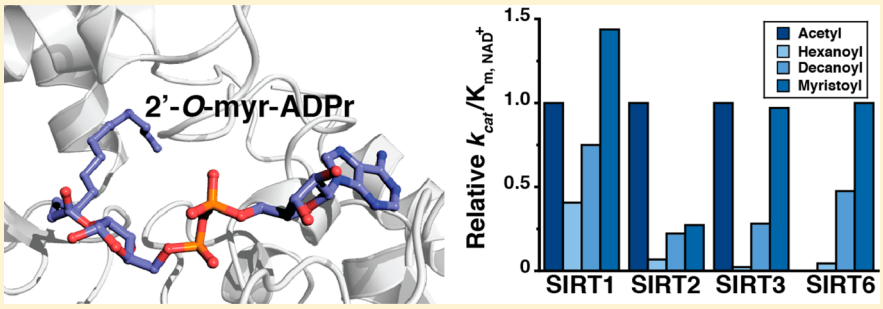

ABSTRACT: Acylation of lysine is an important protein modification regulating diverse biological processes. It was recently demonstrated that members of the human Sirtuin family are capable of catalyzing long chain deacylation, in addition to the well-known NAD$^+$-dependent deacetylation activity [Feldman, J. L., Baeza, J., and Denu, J. M. (2013) *J. Biol. Chem. 288*, 31350−31356]. Here we provide a detailed kinetic and structural analysis that describes the interdependence of NAD$^+$-binding and acyl-group selectivity for a diverse series of human Sirtuins, SIRT1−SIRT3 and SIRT6. Steady-state and rapid-quench kinetic analyses indicated that differences in NAD$^+$ saturation and susceptibility to nicotinamide inhibition reflect unique kinetic behavior displayed by each Sirtuin and depend on acyl substrate chain length. Though the rate of nucleophilic attack of the 2′-hydroxyl on the C1′-*O*-alkylimidate intermediate varies with acyl substrate chain length, this step remains rate-determining for SIRT2 and SIRT3; however, for SIRT6, this step is no longer rate-limiting for long chain substrates. Cocrystallization of SIRT2 with myristoylated peptide and NAD$^+$ yielded a co-complex structure with reaction product 2′-*O*-myristoyl-ADP-ribose, revealing a latent hydrophobic cavity to accommodate the long chain acyl group, and suggesting a general mechanism for long chain deacylation. Comparing two separately determined co-complex structures containing either a myristoylated peptide or 2′-*O*-myristoyl-ADP-ribose indicates there are conformational changes at the myristoyl−ribose linkage with minimal structural differences in the enzyme active site. During the deacylation reaction, the fatty acyl group is held in a relatively fixed position. We describe a kinetic and structural model to explain how various Sirtuins display unique acyl substrate preferences and how different reaction kinetics influence NAD$^+$ dependence. The biological implications are discussed.

Mammalian Sirtuins (SIRT1−SIRT7) are a family of nicotinamide adenine dinucleotide (NAD$^+$)-dependent protein deacylases implicated in a wide range of cellular processes. The physiological importance of Sirtuins has spurred interest in elucidating their catalytic properties, substrates, and molecular functions. Beyond ε-amino deacetylation of lysine residues, which was the first established activity attributed to these enzymes, recent *in vitro* evidence indicates that many Sirtuins catalyze longer chain deacylations, including the removal of hexanoyl, octanoyl, decanoyl, dodecanoyl, myristoyl, and palmitoyl groups.[1,2] The results broaden the acylation landscape targeted by Sirtuins and might explain the broad diversity in biological functions. However, a detailed kinetic and structural understanding of catalytic deacylation activities is lacking.

Protein acylation is emerging as a potential cellular control mechanism, and Sirtuins play a major role in regulating acylation status.[3] In addition to acetyl-CoA, other abundant cellular acyl-CoAs serve as acyl donor molecules for the modification of lysine residues. Acyl-CoAs are derived from carbohydrate, protein, and fatty acid metabolism; therefore, their abundance is dictated by the metabolic status of the cell.[4]

Received: February 13, 2015
Revised: April 16, 2015
Published: April 21, 2015

DOI: 10.1021/acs.biochem.5b00150
Biochemistry 2015, 54, 3037−3050

Increased concentrations of reactive acyl-CoAs may drive protein acylation, as previously indicated with acetyl-CoA in yeast and acetyl phosphate in *Escherichia coli*.[5−7] Recent *in vivo* studies identified a series of short and medium chain acyl groups (propionyl, butyryl, succinyl, glutaryl, malonyl, and crotonyl) as post-translational modifications of lysine residues in histone and non-histone proteins located in multiple cellular compartments, including the nucleus and mitochondria.[8−15] Furthermore, these studies found that mitochondrially localized SIRT5 could catalyze desuccinylation, demalonylation, and deglutarylation *in vitro*, and mice lacking SIRT5 displayed global increases in the numbers of these modifications.[9,14,16] SIRT6, a nuclear localized Sirtuin with poor *in vitro* deacetylase activity, was recently established as a lysine demyristoylase *in vitro* and *in vivo*, acting to demyristoylate TNFα.[1,2] Providing further *in vivo* evidence of the prevalence of longer (>C6) chain acylations is difficult as traditional methods for identifying and localizing these modifications, including immunoenrichment using modification specific antibodies and mass spectrometry, have yet to be optimized for this purpose. However, Jiang et al. identified a number of cellular acylated proteins using a fluorescent reporter-based assay, providing additional evidence that these modifications exist *in vivo*.[2]

Previously, we showed that SIRT1−SIRT6 could all catalyze long chain deacylations, but with varying degrees of specificity and efficiency.[1] The mechanistic basis underlying these unique deacylation profiles was not investigated. In particular, the links between NAD^+ dependence and the nature of the acyl group are unclear. NAD^+ metabolism is known to affect the cellular functions of some Sirtuins;[17] however, whether alterations in NAD^+ binding are dependent on the acyl substrate and how diverse acyl groups affect the various catalytic steps remain unknown.

Here, we performed a series of kinetic and structural studies to explain the unique deacylation signatures for human Sirtuins SIRT1−SIRT3 and SIRT6. These human Sirtuins exist in distinct subcellular compartments and represent two phyla of Sirtuin enzymes.[18] Using acetylated, hexanoylated, deconylated, and myristoylated peptides as substrates, we find the K_m for NAD^+ and the sensitivity to nicotinamide inhibition are dependent on the Sirtuin, as well as the chain length of the acylated substrate. Our results show that SIRT1−SIRT3 and SIRT6 exhibit varying catalytic efficiencies and substrate preferences among the various acyl modifications. Pre-steady-state kinetic analysis provides insight into the microscopic rate constants that contribute to k_{cat}, $k_{cat}/K_{m,NAD}$, and $K_{m,NAD}$ and reveal differences between Sirtuins that are not observed in the macroscopic rate constants. The rate of nucleophilic attack of the 2′-hydroxyl on the C1′-*O*-alkylimidate intermediate varies with acyl substrate chain length and remains the rate-determining step for SIRT2 and SIRT3. However, with long chain substrates, this step is no longer rate-limiting for SIRT6. Furthermore, we cocrystallized SIRT2 with myristoylated peptide, and with myristoylated peptide and NAD^+, which allowed direct observation of the product. Through an induced fit mechanism, conformational changes in the zinc-binding domain and helix bundle region create a cavity to accommodate the acyl chain. Comparison of the crystal structures of SIRT2 in complex with myristoylated peptide and with 2′-*O*-myristoyl-ADP-ribose reveals the conformational changes in the myristoyl group occur near the myristoyl−ribose linkage, while the fatty acyl group is held in a fixed position during the deacylation reaction in the hydrophobic cavity suited for binding the acyl chain. The kinetic and structural characterization provide a more complete understanding of the mechanisms that control Sirtuin deacylase activity. In addition, these results may aid in the interpretation of cellular studies and allow for the design of rational small molecule regulators of Sirtuin activity.

EXPERIMENTAL PROCEDURES

Expression and Purification of Recombinant Human SIRT1−SIRT3 and SIRT6. His-tagged SIRT1−SIRT3 and SIRT6 were overexpressed in *E. coli* strain BL21 (DE3). Overexpression was initiated by growing cells to an OD_{600} of 0.6−0.8 at 37 °C. To induce expression, 0.5 mM isopropyl 1-thio-D-galactopyranoside (IPTG) was added and cells were grown at room temperature for 6 h (SIRT1 and SIRT2) or 18 h. Cells were harvested by centrifugation and stored at −80 °C. SIRT1,[19] SIRT2,[20] SIRT3,[21] and SIRT6[22] were purified as reported previously. Protein concentrations were determined by the Bradford assay.

Synthesis and Analysis of the Acyl H3K9 Peptides. Peptides corresponding to residues 4−17 of histone H3 (acetyl, Ac-KQTARKacSTGGKAPR-WW-NH_2; hexanoyl, Ac-KQTAR-KhexSTGGKAPR-WW-NH_2; decanoyl, Ac-KQTARK-decSTGGKAPR-WW-NH_2; and myristoyl, Ac-KQTARK-myrSTGGKAPR-WW-NH_2) were synthesized by standard solid phase peptide synthesis on a Prelude instrument (Protein Technologies). The side chain of lysine 9 was protected with a 1-(4,4-dimethyl-2,6-dioxocyclohex-1-ylidene)-3-methylbutyl (ivDde) group. Following synthesis, the amino terminus was acetylated using acetic anhydride. The ivDde group was then removed by incubating the peptide resin with 4% hydrazine in dimethylformamide (DMF) for 10 min. The liquid was extracted, and the incubation was repeated a total of seven times. The peptide resin was then incubated with various acyl anhydrides for 2 × 20 min. The acylation solutions contained 528 mM acyl anhydride (acetic, hexanoic, decanoic, and myristic) in toluene. The resin was then washed with DMF followed by dichloromethane (DCM). The peptides were cleaved with a mixture of trifluoroacetic acid (TFA), 5% thioanisole, and 2.5% ethanedithiol. The cleaved peptides were then precipitated in ice-cold ether and lyophilized. The peptides were purified over a preparative C18 high-performance liquid chromatography (HPLC) column. The chromatographic purity of the peptide was determined to be ≥95%, and mass spectrometric analysis on a Bruker REFLEX II MALDI-TOF (matrix-assisted laser desorption ionization time-of-flight) instrument confirmed the identification of the peptide. The acetylated peptide was dissolved in H_2O, and the myristoylated and deconylated peptides were dissolved in 50% DMSO. Two tryptophan residues were added to the C-terminus for quantification at 280 nm.

Determination of Kinetic Parameters for Sirtuin-Dependent Deacylation. Deacylation reactions were analyzed by reversed phase HPLC on a Kinetex C18 column (100 Å, 100 mm × 4.6 mm, 2.6 μm, Phenomenex) by monitoring the formation of the deacylated product at 214 nm. Sirtuin (0.2 μM) or 0.5 μM SIRT6 was incubated with 2.5−1000 μM NAD^+, saturating acetyl-lysine, hexanoyl-lysine, decanoyl-lysine, or myristoyl-lysine in 20 mM sodium phosphate (pH 7.5) at 37 °C. To ensure saturating concentrations of acyl-peptide substrates, approximate K_m values for acyl-peptide and the concentration required to saturate the reaction were experimentally determined. The approximate $K_{m,acyl\text{-}peptide}$ values for the Sirtuins studied were in the low micromolar (<1−20 μM)

DOI: 10.1021/acs.biochem.5b00150
Biochemistry 2015, 54, 3037−3050

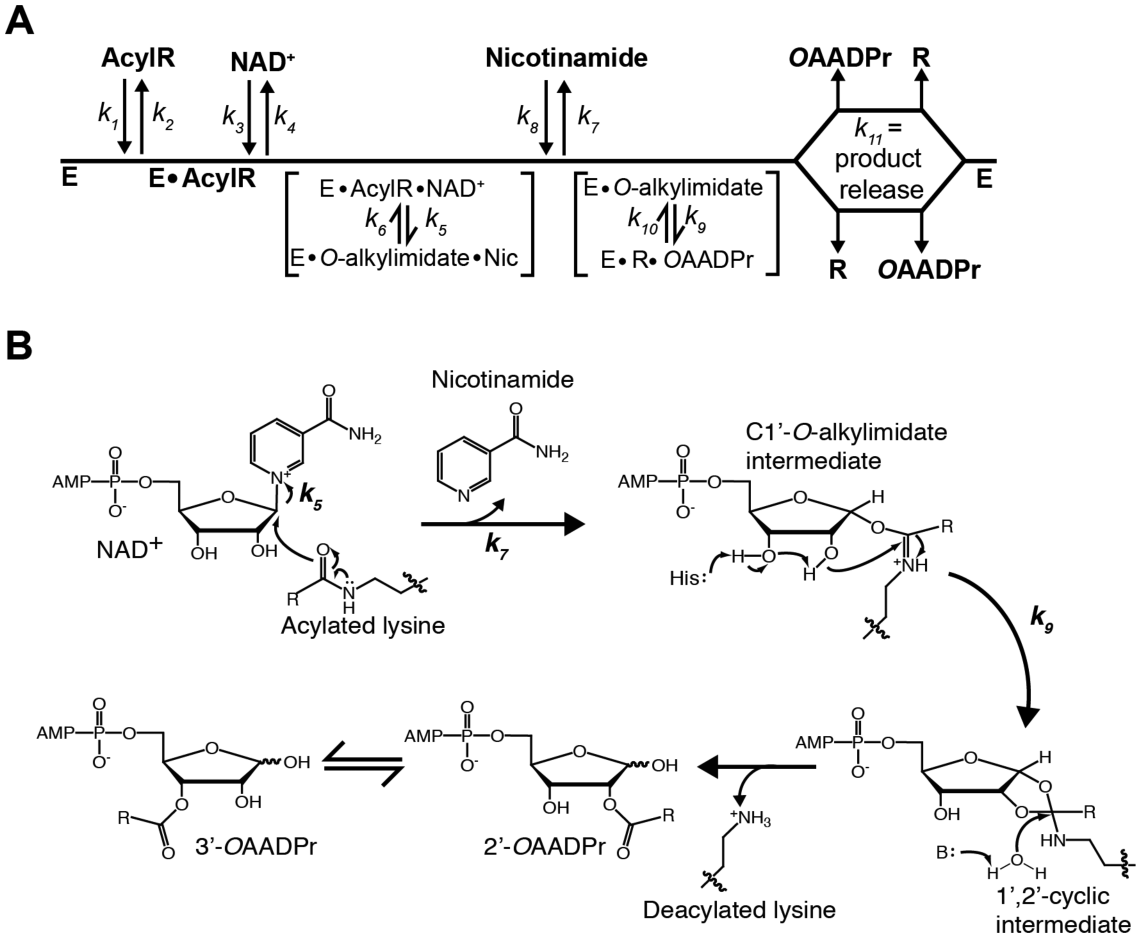

Figure 1. Proposed Sirtuin deacylation mechanism and kinetic scheme. (A) Sirtuin enzymes follow a sequential mechanism in which both acylated substrate (AcylR) (k_1) and NAD$^+$ (k_3) bind prior to any catalytic step. SIRT1−SIRT3 must bind AcylR prior to NAD$^+$, while SIRT6 is the only mammalian Sirtuin capable of binding AcylR or NAD$^+$ in random order. A ternary complex is formed, followed by nicotinamide formation (k_5) and release (k_7), and transfer of the acyl group from AcylR to ADP-ribose (k_9). Deacylated substrate (R) and *O*-acyl-ADPr (*O*AADPr) are randomly released (k_{11}). (B) Proposed deacylation mechanism. Nucleophilic addition of the acyl oxygen on C1′ of the nicotinamide ribose forms the C1′-*O*-alkylimidate intermediate. A conserved histidine residue in the active site activates the 2′-hydroxyl group of NAD$^+$ ribose. The activated hydroxyl attacks the *O*-alkylimidate carbon to afford the 1′,2′-cyclic intermediate. A base-activated water molecule attacks the cyclic intermediate, resulting in the formation of deacylated lysine and *O*AADPr. Rate constants are indicated.

range and below the detection limit of the HPLC system where accurate quantitation is possible. Reactions were quenched with TFA at various time points and mixtures centrifuged at 21000*g* for 5 min. Time points were chosen such that all reactions remained within the steady-state initial velocity during their courses. Deacetylation reactions were analyzed using a gradient of 33 to 100% B (30% acetonitrile with 0.02% TFA) over 20 min at a rate of 1.4 mL min^{-1}. Dehexanoylation, dedecanoylation, and demyristoylation reactions were analyzed using a gradient from 3 to 100% B (acetonitrile with 0.02% TFA) over 10 min at a rate of 1.6 mL min^{-1}. The product and substrate peaks were quantified, rates of deacylation determined, and the data fitted to the Michaelis−Menten equation. Three independent experiments were performed for each Sirtuin−acyl-substrate pair. The averages of the three experiments were plotted and fitted to obtain $K_{m,NAD}$, $k_{cat}/K_{m,NAD}$, and k_{cat}. Error bars represent the standard deviation of the mean.

Steady-State Kinetic Data Analysis. To demonstrate the effects of reaction kinetics on the acyl-substrate-dependent Sirtuin activities in terms of the microscopic rate constants, we used the net rate constant method of Cleland[23] to derive the initial velocity equation for the proposed kinetic mechanism (Figure 1A). The kinetic analysis was performed at a saturating acyl-peptide substrate concentration, forcing all free enzyme into an enzyme−acyl-peptide substrate complex. Thus, k_1 and k_2 do not contribute to the initial velocity measurements. On the basis of the steady-state approximation, k_8 (rebinding of nicotinamide) will be equal to zero, and assuming a random product release of *O*AADPr and deacylated peptide,[24] we defined a single kinetic constant, k_{11}, to encompass the rate of product release, allowing the equation to be simplified to (eq 1)

$$\frac{v}{E_t} = \left(k_3k_5k_7k_9k_{11}[\mathrm{NAD^+}]\right) \Big/ \Big[k_9k_{11}(k_4k_6 + k_4k_7 + k_5k_7) + k_3[\mathrm{NAD^+}](k_6k_9k_{11} + k_7k_9k_{11} + k_5k_9k_{11} + k_5k_7k_{10} + k_5k_7k_{11} + k_5k_7k_9)\Big] \quad (1)$$

The rate of nicotinamide release (k_7) is believed to be fast relative to all other steps. Using Figure 1A as the kinetic model, as well as the previous assumptions, we can derive the equation for k_{cat} (eq 2) and $k_{cat}/K_{m,NAD}$ (eq 3), which are equal to

DOI: 10.1021/acs.biochem.5b00150
Biochemistry 2015, 54, 3037−3050

$$k_{cat} = \frac{k_5 k_9 k_{11}}{k_5 k_9 + k_5 k_{10} + k_5 k_{11} + k_9 k_{11}} \quad (2)$$

$$\frac{k_{cat}}{K_{m,NAD}} = \frac{k_3 k_5}{k_4 + k_5} \quad (3)$$

The k_{cat} value reflects chemical catalysis (k_5, k_9, and k_{10}) as well as deacylated substrate and *O*AADPr release (k_{11}). However, because turnover is often controlled by a single slow step, the k_{cat} expression will likely simplify to a single rate constant (either k_5, k_9, k_{10}, or k_{11}). The k_{cat}/K_m value for NAD^+ encompasses both NAD^+ binding (k_3 and k_4) and NAD^+ cleavage (k_5). The k_{cat}/K_m measures the apparent rate of enzyme capture of the substrate to form a productive complex destined to form products and reflects enzyme activity at low substrate levels.[25]

The K_m value for NAD^+ is the ratio of k_{cat} and $k_{cat}/K_{m,NAD}$ and is the steady-state Michaelis constant for the Sirtuin−NAD^+−acyl-substrate ternary complex. The K_m reflects both binding and catalysis and is equal to (eq 4)

$$K_{m,NAD} = \frac{k_9 k_{11}(k_4 + k_5)}{k_3(k_9 k_{11} + k_5 k_{10} + k_5 k_{11} + k_5 k_9)} = \frac{k_{cat}(k_4 + k_5)}{k_3 k_5} \quad (4)$$

A change in K_m for NAD^+ can be due to a change in k_{cat}, k_5, or NAD^+ binding (change in k_3 or k_4) (Figure 1A).

Rapid-Quench Analysis for Determining the Rates of Product Formation. The rates of nicotinamide and deacylated peptide formation were determined under single-turnover conditions using a Hi-Tech RQF-63 rapid-quench flow device (Hi-Tech Scientific, Bradford-on-Avon, U.K.) as previously described.[24] Single-turnover reaction mixtures for SIRT2 contained 400 μM NAD^+, 2.5 μM acyl-peptide, and 12 μM SIRT2 in 20 mM potassium phosphate (pH 7.5) at 37 °C. Reactions were monitored from 100 to 30000 ms and were quenched with TFA that was added to a final concentration of 1% on the rapid-quench flow system. Single-turnover reaction mixtures for SIRT3 contained 2.5 μM acyl-peptide and varying NAD^+ concentrations depending on the acyl-substrate as follows; 1 mM NAD^+ (acetyl peptide), 2 mM NAD^+ (hexanoyl peptide), or 600 μM NAD^+ (decanoyl and myristoyl peptides) and 12 μM SIRT3 in 20 mM potassium phosphate (pH 7.5) at 37 °C. Reactions were monitored from 100 to 30000 ms and were quenched with TFA that was added to a final concentration of 1% on the rapid-quench flow system. Single-turnover reaction mixtures for SIRT6 contained 300 μM NAD^+, 5 μM acyl-peptide, and 18 μM SIRT6 in 20 mM potassium phosphate (pH 7.5) at 37 °C. Reactions were monitored from 5 to 180 s and were manually quenched with TFA that was added to a final concentration of 1%. For reaction mixtures containing hexanoylated, decanoylated, and myristoylated substrates, nicotinamide, NAD^+, deacylated product, and acylated substrate were analyzed by reversed phase HPLC using a gradient from 0 to 4% B (acetonitrile with 0.02% TFA) over 12.5 min followed by a gradient from 20 to 100% B over 30 min on a Vydac 201SP104 C18 small pore column. For reaction mixtures containing the acetylated substrate, solvent B consisted of 30% acetonitrile and 0.02% TFA, and the same gradient was used for separation. Product and reactant peaks were quantified. The concentration of nicotinamide was determined on the basis of a standard curve measured at 260 nm. The concentration of deacylated peptide was determined as described above for steady-state measurements. To obtain the first-order rate constant (k), the plot of product concentration formed over time was fit to the single-exponential equation $P = [S]_0(1 - e^{-kt})$, where P is the concentration of product formed, $[S]_0$ is the initial concentration of the limiting substrate, and t is the reaction time.[26] For all acyl substrates, complete conversion of the peptide was not attainable. Therefore, to fit these analogues, $[S]_0$ was set to 2.5 μM.

Nicotinamide Inhibition Assay. Sirtuin (0.2 μM) or 0.5 μM SIRT6 was incubated with saturating NAD^+ (SIRT1, 500 μM for acetyl, 300 μM for long chain; SIRT2, 500 μM for acetyl, 300 μM for long chain; SIRT3, 500 μM for acetyl, 600 μM for long chain; SIRT6, 800 μM for hexanoyl, 300 μM for decanoyl, 300 μM for myristoyl) and saturating acyl-lysine peptides (SIRT1, 50 μM for acetyl, 40 μM for hexanoyl, 20 μM for decanoyl, 15 μM for myristoyl; SIRT2, 50 μM for acetyl, 15 μM for hexanoyl, 15 μM for decanoyl, 15 μM for myristoyl; SIRT3, 70 μM for acetyl, 70 μM for hexanoyl, 20 μM for decanoyl, 15 μM for myristoyl; SIRT6, 200 μM for hexanoyl, 50 μM for decanoyl, 50 μM for myristoyl) in the presence of 0−1.5 mM nicotinamide in 20 mM sodium phosphate (pH 7.5) at 37 °C. Reactions were quenched and analyzed as described above. The data were fitted to the Langmuir isotherm equation to determine the half-maximal inhibitory concentration (IC_{50})[27]

$$\text{fractional activity} = \frac{1}{1 + \frac{[I]}{IC_{50}} + x} \quad (5)$$

where [I] is the concentration of the inhibitor and x is the fractional activity minimum. Each reaction was performed two or three times, and the average rate was plotted. Error bars represent the standard deviation of the mean.

Crystallization and Determination of the Structure of SIRT2. GST-tagged SIRT2 was overexpressed in *E. coli* strain BL21 (DE3) using the same method that was used for His-SIRT2 described above and purified using Glutathione Sepharose 4B resin (GE Healthcare) according to the manufacturer's protocol. After thrombin digestion, SIRT2 was further purified by ion exchange chromatography [Resource Q column (GE Healthcare), 20 mM Tris-HCl (pH 8.0), and 0−1 M NaCl]. Sodium dodecyl sulfate−polyacrylamide gel electrophoresis was used to pool SIRT2-containing fractions. Myristoylated peptides [TNF-αK20myr (LPKKmyrTGG) and H3K9myr (TARKmyrSTG)] were used for crystallization (purchased from Toray Research Center). SIRT2 (15−20 mg/mL) and myristoylated peptide (final concentration of 1 mM) were mixed, and crystallization screening using commercially available kits (Hampton Research) was performed. Each drop consisting of 0.4 μL of a protein/peptide mixture and 0.4 μL of reservoir solution was equilibrated against 80 μL of reservoir solution at 293 K by the sitting-drop vapor-diffusion method. Crystals for X-ray crystallography were obtained using 20−25% PEG3350 and 0.2 M potassium formate for the H3K9myr peptide complex, or 0.2 M ammonium acetate for the TNF-αK20myr peptide complex. We also crystallized SIRT2 with myristoylated peptide and NAD^+ to obtain a 2′-*O*-acyl ADP ribose structure, and crystals were obtained under a condition using 20−25% PEG2000 monomethyl ether and 0.1 M BisTris (pH 6.0−6.5). Crystals

DOI: 10.1021/acs.biochem.5b00150
Biochemistry 2015, 54, 3037−3050

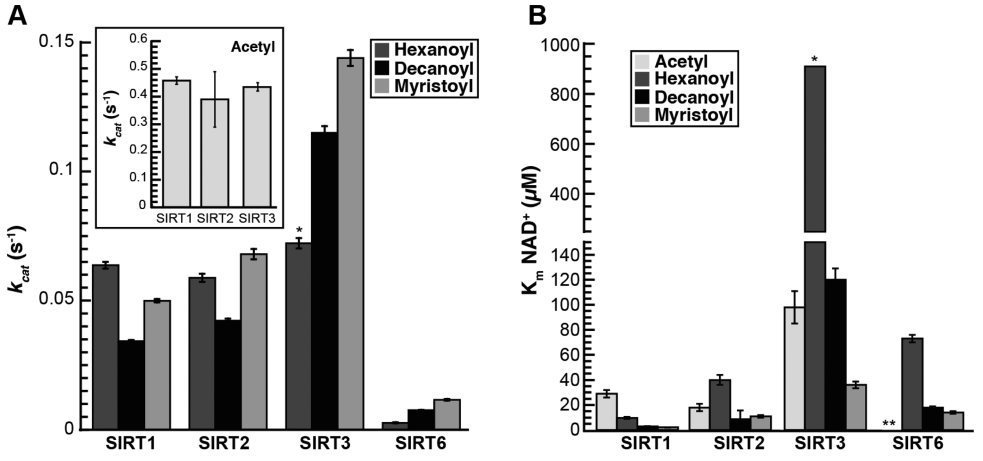

	Acetyl	Hexanoyl	Decanoyl	Myristoyl
SIRT1	$4.6x10^{-1} \pm 1x10^{-2}$	$6.4x10^{-2} \pm 1x10^{-3}$	$3.4x10^{-2} \pm 1x10^{-3}$	$5.1x10^{-2} \pm 1x10^{-3}$
SIRT2	$3.9x10^{-1} \pm 1x10^{-2}$	$5.9x10^{-2} \pm 2x10^{-3}$	$4.2x10^{-2} \pm 1x10^{-3}$	$6.8x10^{-2} \pm 2x10^{-3}$
SIRT3	$3.3x10^{-1} \pm 1x10^{-2}$	$7.2x10^{-2} \pm 2x10^{-3*}$	$1.2x10^{-1} \pm 3x10^{-3}$	$1.2x10^{-1} \pm 2x10^{-3}$
SIRT6	n.d.	$2.7x10^{-3} \pm 2x10^{-4}$	$7.6x10^{-3} \pm 1x10^{-4}$	$1.2x10^{-2} \pm 3x10^{-4}$

	Acetyl	Hexanoyl	Decanoyl	Myristoyl
SIRT1	29 ± 3	9.7 ± 0.8	3.0 ± 0.2	2.2 ± 0.1
SIRT2	18 ± 3	40 ± 4	8.7 ± 0.7	11 ± 1
SIRT3	98 ± 13	>910*	120 ± 9	36 ± 2
SIRT6	n.d.	72 ± 2	19 ± 1	14 ± 1

Figure 2. k_{cat} and $K_{m,NAD}$ for SIRT1−SIRT3 and SIRT6 deacylation reactions. (A) k_{cat} values. The inset shows k_{cat} values for acetylated substrate plotted separately for the sake of clarity. Calculated k_{cat} values determined from nonlinear regression fits to the Michaelis−Menten equation shown below. (B) K_m for NAD^+. Calculated $K_{m,NAD}$ values determined from nonlinear regression fits to the Michaelis−Menten equation. One asterisk indicates an estimate for SIRT3 resulting from an inability to saturate the reaction mixture with NAD^+, and two asterisks indicate the $K_{m,NAD}$ with acetylated peptide for SIRT6 was not measured due to the prohibitively high peptide substrate concentration necessary to saturate the reaction ($n \geq 3$, ±standard deviation of the mean).

were grown in a week. Crystals were frozen by liquid nitrogen, using 10% 2-methyl-2,4-pentanediol as a cryoprotectant. X-ray diffraction data were collected at 100 K in a nitrogen gas stream at synchrotron beamlines PF-BL5A, PF-BL17A, and PF-AR NW12A at Photon Factory, KEK (Proposal 2013G674). Data were processed with the programs denzo and scalepack from the HKL package[28] (HKL Research, Charlottesville, VA). The structures were determined by molecular replacement using Molrep.[29] The SIRT2 structure in the apo form (PDB entries 1J8F and 3ZGO) was used as a search model. Refinement and model building were performed with REFMAC5[30] and Coot.[31] The geometric quality of the model was assessed with MolProbity.[32] Data collection and refinement statistics are listed in Table 2. Atomic coordinates and structure factors have been deposited in the PDB [entries 4Y6L for human SIRT2 in complex with myristoylated peptide (H3K9myr), 4Y6O for human SIRT2 in complex with myristoylated peptide (TNF-αK20myr), and 4Y6Q for human SIRT2 in complex with 2-*O*-myristoyl-ADP-ribose]. We also re-refined the SIRT6 coordinates in complex with a myristoylated peptide (PDB entry 3ZG6)[2] and used the re-refined coordinates throughout this paper.

RESULTS

Catalytic Efficiency and NAD^+ Binding Kinetics of Human Sirtuin Enzymes with Various Acyl-Substrates. Our previous results indicate that each Sirtuin has a unique acyl substrate specificity pattern;[1] however, the molecular basis for these patterns was not investigated. The initial characterization of the deacylation activity was performed at a saturating peptide concentration (5 mM) and a limiting NAD^+ concentration, suggesting differences in acyl-substrate reactivity could be due to alterations in NAD^+ binding and/or catalysis. To investigate a kinetic model that can explain isoform specific human Sirtuin deacylation activity, we determined the steady-state kinetic parameters k_{cat} (eq 2), $k_{cat}/K_{m,NAD}$ (eq 3), and $K_{m,NAD}$ (eq 4) for SIRT1−SIRT3 and SIRT6, using four different acyl-group substrates representing a range of short, medium, and long acyl chain lengths. Analyzed together, these kinetic parameters provide insight into the Sirtuin kinetic mechanism (Figure 1A,B) and an understanding of the relationship between the deacylation activities of diverse human Sirtuins and NAD^+ binding.

Human Sirtuins were overexpressed in *E. coli* and purified as previously described.[19−22] Sirtuin enzyme (0.2 or 0.5 μM SIRT6) was incubated with a histone H3 lysine 9 (H3K9) acetylated, hexanoylated (C6), decanoylated (C10), or myristoylated (C14) peptide at saturating concentrations, with varying NAD^+ levels. To interrogate only the effect of the acyl group on catalysis, the same peptide sequence, representing amino acids 4−17 of histone H3 with two tryptophan residues added for peptide quantitation (Ac-KQTARKacylSTGGKAPR-WW), was used in all assays. Steady-state deacylation rates were determined using an HPLC-based assay that monitors the formation of deacylated product.[1]

Data from three independent experiments were fitted to the Michaelis−Menten equation (Figure S1 of the Supporting Information), and the resulting average k_{cat}, $K_{m,NAD}$, and $k_{cat}/K_{m,NAD}$ values were compared (Figures 2 and 3). A $K_{m,NAD}$ for SIRT6 with the acetylated substrate was not determined because of the prohibitively high concentration of acetylated peptide needed to perform the assay under saturating peptide conditions (estimated to be nearly 4.5 mM[1]). Additionally, the hexanoylated peptide was a poor substrate for SIRT3, and we were unable to saturate the reaction with NAD^+. Therefore, only the $k_{cat}/K_{m,NAD}$ value was accurately obtained for this reaction, resulting in estimates for $K_{m,NAD}$ and k_{cat}.

SIRT1−SIRT3 displayed the highest k_{cat} with the acetylated substrate (Figure 2A, inset), while having similar k_{cat} values among the hexanoylated, decanoylated, and myristoylated substrates (Figure 2A). The k_{cat} values for SIRT6 increase

DOI: 10.1021/acs.biochem.5b00150
Biochemistry 2015, 54, 3037−3050

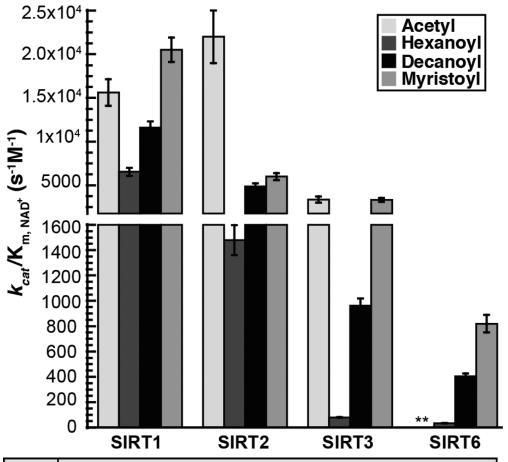

	Acetyl	Hexanoyl	Decanoyl	Myristoyl
SIRT1	$1.6x10^4 \pm 2x10^3$	$6.5x10^3 \pm 5x10^2$	$1.2x10^4 \pm 7x10^2$	$2.3x10^4 \pm 1x10^3$
SIRT2	$2.2x10^4 \pm 3x10^3$	$1.5x10^3 \pm 1x10^2$	$4.9x10^3 \pm 4x10^2$	$6.0x10^3 \pm 4x10^2$
SIRT3	$3.4x10^3 \pm 3x10^2$	79 ± 2	$9.6x10^2 \pm 6x10^2$	$3.3x10^3 \pm 2x10^2$
SIRT6	n.d.	37 ± 1	$3.9x10^2 \pm 2x10^1$	$8.2x10^2 \pm 7x10^1$

Figure 3. $k_{cat}/K_{m,NAD}$ for SIRT1−SIRT3 and SIRT6 deacylation reactions. $k_{cat}/K_{m,NAD}$ determined for SIRT1−SIRT3 and SIRT6 in the presence of acetyl-, hexanoyl-, decanoyl-, and myristoyl-lysine H3K9 peptides. Calculated parameters determined from nonlinear regression fits to the Michaelis−Menten equation. Two asterisks indicate $k_{cat}/K_{m,NAD}$ with acetylated peptide for SIRT6 was not measured because of the prohibitively high peptide substrate concentration necessary to saturate the reaction ($n \geq 3$, ±standard deviation of the mean).

nearly 4-fold as the chain length increases from hexanoyl to myristoyl (Figure 2A and Table S1 of the Supporting Information). The $K_{m,NAD}$ values for SIRT1 decrease as the length of the acyl group increases from acetyl to myristoyl (Figure 2B and Table S1 of the Supporting Information). The $K_{m,NAD}$ values for SIRT2 and SIRT3 are more varied; however, the $K_{m,NAD}$ does decrease as the chain length increases from hexanoyl to myristoyl, similar to the decrease in $K_{m,NAD}$ observed with SIRT6 (Figure 2B and Table S1 of the Supporting Information). For all Sirtuins tested, $k_{cat}/K_{m,NAD}$ increased as the acyl chain length increased from hexanoyl (C6) to myristoyl (C14) (Figure 3). With respect to $k_{cat}/K_{m,NAD}$ values for SIRT2, there was a significant preference for the acetylated substrate, where the rates were 4−15 times higher than that of other acyl-substrates. The highest $k_{cat}/K_{m,NAD}$ values for SIRT3 were observed with the acetylated and myristoylated substrates and were 42 and 3.5 times higher than the rates with the hexanoylated and decanoylated substrates, respectively (Table S1 of the Supporting Information). SIRT6 preferred myristoylated and decanoylated substrates relative to a hexanoyl substrate, with $k_{cat}/K_{m,NAD}$ values being 22 and 10.5 times higher, respectively. Although $k_{cat}/K_{m,NAD}$ values with SIRT1 are similar among all acyl-substrates analyzed, SIRT1 displayed a decreased rate with the hexanoylated substrate relative to acetylated, decanoylated, and myristoylated substrates. Together, the results indicate that while each Sirtuin displays varied specificity and catalytic efficiency for deacylation, there is an interdependence between the acylated substrate and NAD^+ capture ($k_{cat}/K_{m,NAD}$).

Nicotinamide Inhibition Analysis. Nicotinamide is the first product released during the deacylation reaction and exhibits noncompetitive inhibition with respect to NAD^+ and acylated substrate.[24] Previous studies demonstrated that free radiolabeled nicotinamide is capable of rebinding the active site and intercepting the *O*-alkylimidate intermediate to re-form NAD^+ through nicotinamide exchange.[33] The slower the second chemical step of the reaction (k_9) or rate of association and dissociation of nicotinamide (k_7 and k_8, respectively), the more susceptible the enzyme is to nicotinamide inhibition (Figure 1A,B). To investigate the effect of the acyl substrate on the ability of nicotinamide to inhibit deacylation, we determined the IC_{50} of nicotinamide with SIRT1−SIRT3 and SIRT6 in the presence of acetylated, hexanoylated, decanoylated, and myristoylated substrates. We found that the IC_{50} of nicotinamide varied with the Sirtuin and acyl-substrate analyzed (Figure 4).

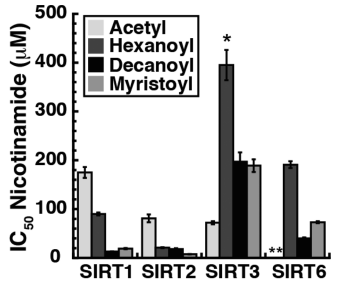

	Acetyl	Hex	Dec	Myr
SIRT1	175 ± 11	90 ± 3	13 ± 1	19 ± 1
SIRT2	80 ± 8	21 ± 1	18 ± 2	8 ± 1
SIRT3	72 ± 3	400 ± 30*	200 ± 20	190 ± 13
SIRT6	n.d.	184 ± 8	45 ± 2	73 ± 3

Figure 4. Nicotinamide IC_{50} values. SIRT1−SIRT3 and SIRT6 display varied susceptibilities to nicotinamide inhibition depending upon acyl-substrate ($n \geq 2$, ±standard deviation). One asterisk indicates that because of the high K_m for NAD^+ in the presence of the hexanoylated peptide (>910 μM), the assay was performed in the presence of 800 μM NAD^+. Two asterisks indicate that the nicotinamide IC_{50} for SIRT6 in the presence of acetylated peptide was not measured because of the prohibitively high peptide substrate concentration necessary to saturate the reaction.

Steady-state nicotinamide inhibition assays were conducted at fixed, saturating concentrations of acetylated, hexanoylated, decanoylated, or myristoylated peptides, saturating NAD^+, with Sirtuin concentrations (0.2 or 0.5 μM SIRT6), and nicotinamide concentrations varying 0−1500 μM. Reaction rates were quantified and fitted to the Langmuir equation (eq 5) to determine the half-maximal inhibitory concentration (IC_{50}) (Figure S2 of the Supporting Information), and average IC_{50} values of two or three independent experiments were compared (Figure 4). We were unable to measure nicotinamide inhibition for SIRT6 with the acetylated substrate because of the prohibitively high concentration of acetyl-peptide needed for saturation, and the $IC_{50,nicotinamide}$ for SIRT3 with the hexanoylated peptide, a poor SIRT3 substrate, is estimated because of the inability to saturate the reaction with NAD^+. For SIRT1 and SIRT2, the IC_{50} for nicotinamide is the highest for the acetylated substrate and decreases as the acyl chain length increases, following the trends observed in k_{cat} (Figures 2A and 4). Interestingly, SIRT3 and SIRT6 display the greatest susceptibility to nicotinamide inhibition in the presence of the substrate that had the highest k_{cat} (Figures 2A and 4). SIRT3 is more inhibited by nicotinamide with the acetylated substrate than with the longer chain acyl substrates, and SIRT6 is more inhibited by nicotinamide with the myristoylated and decanoylated peptides relative to the hexanoylated substrate

DOI: 10.1021/acs.biochem.5b00150
Biochemistry 2015, 54, 3037−3050

Table 1. Rapid-Quench Rates of Nicotinamide and Deacylated Product Formation[a]

	acetyl	hexanoyl	decanoyl	myristoyl
		Nicotinamide Formation Rate, k_5 (s^{-1})		
SIRT2	$(1.6 \pm 3) \times 10^{-1}$	$2.9 \times 10^{-1} \pm 3 \times 10^{-2}$	$4.3 \times 10^{-1} \pm 6 \times 10^{-2}$	$(9 \pm 2) \times 10^{-1}$
SIRT3	$(3.8 \pm 6) \times 10^{-1}$	$2.8 \times 10^{-1} \pm 5 \times 10^{-2}$	$4.0 \times 10^{-1} \pm 4 \times 10^{-2}$	$7.6 \times 10^{-1} \pm 6 \times 10^{-2}$
SIRT6	ND	$4.4 \times 10^{-3} \pm 6 \times 10^{-4}$	$7.3 \times 10^{-2} \pm 8 \times 10^{-3}$	$1.4 \times 10^{-1} \pm 2 \times 10^{-2}$
		Deacylated Peptide Formation Rate, k_9 (s^{-1})		
SIRT2	$5.3 \times 10^{-1} \pm 6 \times 10^{-2}$	$1.1 \times 10^{-1} \pm 1 \times 10^{-2}$	$9.0 \times 10^{-2} \pm 8 \times 10^{-3}$	$5.3 \times 10^{-2} \pm 5 \times 10^{-3}$
SIRT3	$6.5 \times 10^{-1} \pm 2 \times 10^{-2}$	$(8 \pm 1) \times 10^{-2}$	$1.0 \times 10^{-1} \pm 1 \times 10^{-2}$	$6.5 \times 10^{-2} \pm 6 \times 10^{-3}$
SIRT6	ND	$2.3 \times 10^{-3} \pm 1 \times 10^{-4}$	$3.3 \times 10^{-2} \pm 3 \times 10^{-3}$	$4.2 \times 10^{-2} \pm 4 \times 10^{-3}$

[a]Average rate and standard deviation of two or three independent experiments.

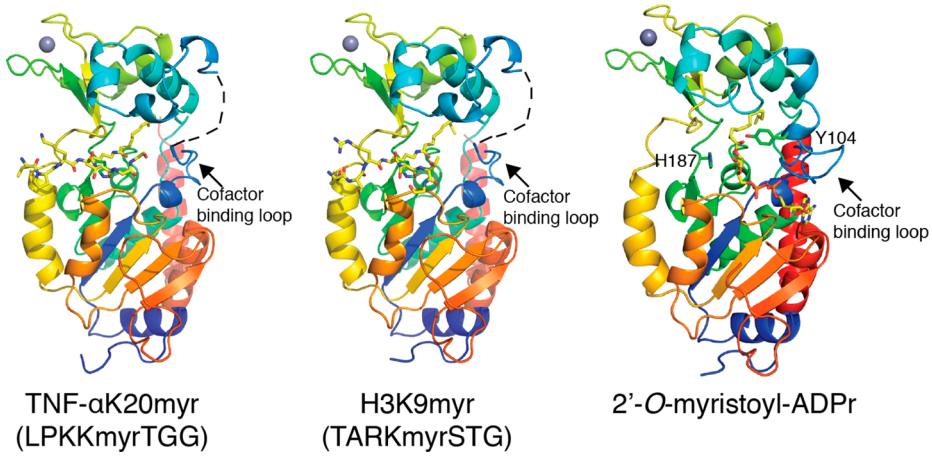

Figure 5. Crystal structure of SIRT2 in complex with TNFα-K20myr, H3K9myr, or 2′-*O*-myristoyl-ADP-ribose. Overall structural features of SIRT2 in the presence of myristoylated substrates or product. The cofactor-binding loop was not visible in the SIRT2−TNFα-K20myr or SIRT2−H3K9myr structures and is shown as a dashed line for the sake of clarity. Also highlighted in the 2′-*O*-myristoyl-ADPr structure are the locations and orientations of Tyr104 and the catalytic histidine, His187.

(Figure 4). The results indicate that in addition to the interdependence between acylated substrate and NAD^+ binding, susceptibility to nicotinamide inhibition is also dependent on the acylated substrate for each Sirtuin.

Rapid-Quench Analysis: Resolving Individual Chemical Steps in Catalysis. The steady-state reaction parameters and nicotinamide inhibition assays suggest differences in catalytic efficiency that result from the use of diverse acyl-substrates are due to both catalysis and NAD^+ binding. Changes in $k_{cat}/K_{m,NAD}$ reflect the rate of the reaction through the first committed step and include both NAD^+ binding and cleavage (Figure 1A and eq 3). In addition, the differences in k_{cat} measured with the various acylated peptides for a given Sirtuin can be due to differences in the rate of the slowest reaction step or can be caused by a change in the rate-limiting step for the entire reaction, for example, from chemistry to product release. To provide mechanistic details about the individual steps involved in catalysis and product formation, and to assess whether the distinct kinetic profiles in our initial velocity analysis could be explained by a change in the rate-limiting step of the reaction, a pre-steady-state, rapid-quench kinetic analysis was performed. This analysis was performed for SIRT2 and SIRT3 with acetylated, hexanoylated, decanoylated, and myristoylated substrates and for SIRT6 with hexanoylated, decanoylated, and myristoylated substrates. SIRT1 was excluded from the analysis because of the co-elution of the high levels of SIRT1 needed for single-turnover analysis and the acylated peptides during HPLC analysis, limiting our ability to accurately quantify deacylated product formation. Assays were performed with limiting acyl-substrate, allowing only a single turnover of the enzyme. Sirtuin enzyme (12 μM SIRT2, 12 μM SIRT3, or 18 μM SIRT6) was incubated with saturating concentrations of NAD^+ and 2.5 μM acyl-peptide or 5 μM acyl-peptide for SIRT6. Under these conditions, all acyl-peptide is assumed to be bound to Sirtuin.[34] At six to eight time points, reactions were rapidly quenched with TFA and nicotinamide, deacylated peptide, and acylated peptide were resolved and quantified by HPLC. To determine rates of nicotinamide (k_5) and deacylated product formation, data from two or three separate experiments per Sirtuin enzyme were fitted to a single exponential (Figure S3 of the Supporting Information). The rate of deacylated product formation represents the rate of nucleophilic attack of the 2′-hydroxyl on the C1′-*O*-alkylimidate intermediate in the second chemical step of the deacylation reaction (k_9). The experiments were in excellent agreement, and the average rates and standard deviations are listed in Table 1. For all enzymes and substrates analyzed, the rate of nicotinamide formation (k_5) exceeded the rate of nucleophilic attack of the 2′-hydroxyl (k_9) (Figure 1B).

Structural Insight into Catalysis of Long Chain Deacylation. To investigate the molecular basis for varied sensitivity to acyl chain length observed in the rate constants and provide insight into the deacylation mechanism as well as the conformational changes the protein, substrates, and products undergo during catalysis, we determined crystal structures of SIRT2 in complex with myristoylated TNF-αK20 or H3K9 substrates at 1.6 Å resolution. To obtain the product complex, we crystallized SIRT2 with myristoylated

DOI: 10.1021/acs.biochem.5b00150
Biochemistry 2015, 54, 3037−3050

Table 2. Data Collection and Refinement Statistics

	TNF-αK20myr	H3K9myr	TNF-αK20myr NAD$^+$
Data Collection			
X-ray source	PF-BL5A	PF-BL5A	PF-BL17A
space group	*P*1	*P*1	$P2_1$
unit cell dimensions			
a (Å)	37.1	37.1	61.2
b (Å)	48.7	48.8	142.3
c (Å)	96.8	97.1	62.6
α (deg)	101.2	101.0	90.0
β (deg)	91.3	91.5	94.3
γ (deg)	112.3	112.0	90.0
wavelength (Å)	1.000	1.000	0.980
resolution (Å)	50.0−1.6 (1.63−1.60)	50.0−1.6 (1.63−1.60)	50−1.85 (1.88−1.85)
no. of unique reflections	77514	79168	90675
completeness (%)[a]	95.7 (92.2)	95.6 (93.6)	98.3 (96.6)
R_{merge} (%)[a]	4.9 (20.8)	2.3 (14.0)	6.3 (64.3)
$I/\sigma(I)$[a]	14.3 (3.2)	38.5 (14.5)	17.0 (1.8)
Wilson *B* factor (Å^2)	10.3	9.8	41.9
Refinement			
resolution range (Å)	20.0−1.6	20.0−1.6	20.0−1.9
no. of reflections	73362	74836	74580
no. of non-hydrogen atoms	5030	4988	9471
R_{work} (%)	21.3	21.7	25.1
R_{free} (%)	24.0	23.7	27.1
rmsd			
bond lengths (Å)	0.007	0.007	0.009
bond angles (deg)	1.291	1.252	1.445
B factor (Å^2)			
protein	16.5	15.2	22.3
substrate/product	26.4	21.5	20.3
waters	20.6	20.7	19.3
Ramachandran plot (%)			
favored region	97.5	97.6	98.1
allowed region	2.0	2.4	1.8
outlier region	0.5	0.0	0.1

[a]Values in parentheses are for the highest-resolution shell.

TNF-αK20 and NAD$^+$ and determined the crystal structure of SIRT2 in complex with 2′-*O*-myristoyl-ADP-ribose, at 1.9 Å resolution (Figure 5 and Table 2). The structures are similar to published SIRT2 structures,[35−37] including a crystal structure published by Teng et al. of SIRT2 in complex with a H3K9myr peptide, which appeared while this work was being reviewed.[38] The overall folds are similar between the substrate and product structures [root-mean-square deviation (rmsd) of 0.7 Å], with the exception of the highly flexible cofactor-binding loop,[39] which shows continuous electron density only in the SIRT2−2′-*O*-myristoyl-ADPr product structure (Figure 5).

Continuous electron density was observed for the myristoyl-lysine residue of the TNF-αK20myr and H3K9myr peptides (Figure 6A,B). Superimposition of the TNF-αK20myr and H3K9myr structures indicates that while there are changes in the orientation of side chain residues in the peptide substrate, the myristoylated lysine residue adopts a nearly identical conformation in the two structures with an rmsd of <0.2 Å (Figure 6C). As in previously published SIRT6−H3K9myr and pfSir2A−H3K9myr structures,[2,40] the aliphatic chain of the myristoylated lysine is located in a hydrophobic pocket (Figure 6D). To examine the conformational differences in SIRT2 that are needed to accommodate the myristoyl chain in the active site compared to a smaller acetyl-like moiety, the SIRT2−H3K9myr structure was superimposed with a crystal structure of SIRT2 bound to an ε-trifluoroacetyl lysine peptide inhibitor.[35] The structures align well (rmsd of 0.4 Å) with the exception of portions of the zinc-binding domain and the helix bundle region (Figure 7A). The greatest differences are observed in α-helices 4 and 6. Amino acids Ile118, Phe119, Phe131, Leu134, and Leu138 shift away from the active site (Figure 7B), suggestive of an induced fit mechanism to accommodate the longer acyl chains. Further, previous structural analysis of SIRT5 in complex with a succinylated substrate identified Tyr-102 and Arg-105, located in α-helix 6, as the amino acids responsible for binding the carboxyl group (Figure 7C),[41] indicating there is likely a common mechanism for substrate binding among the Sirtuins that contain a helix bundle region, including human SIRT1−SIRT5. Superimposition of the SIRT2, SIRT6, and pfSir2A structures reveals the myristoyl chain can bind in a number of different conformations, depending on the hydrophobic pocket and organization of the active site for a given Sirtuin (Figure 7D). As observed in the SIRT6 coordinate file from Jiang et al.[2] (PDB entry 3ZG6), one of the water molecules (A2146 in PDB entry 3ZG6) is in close contact with the myristoylated peptide [<2.2 Å (Figure S4A of the Supporting Information)]. We re-refined the SIRT6 coordinate without the water molecule and

DOI: 10.1021/acs.biochem.5b00150
Biochemistry 2015, 54, 3037−3050

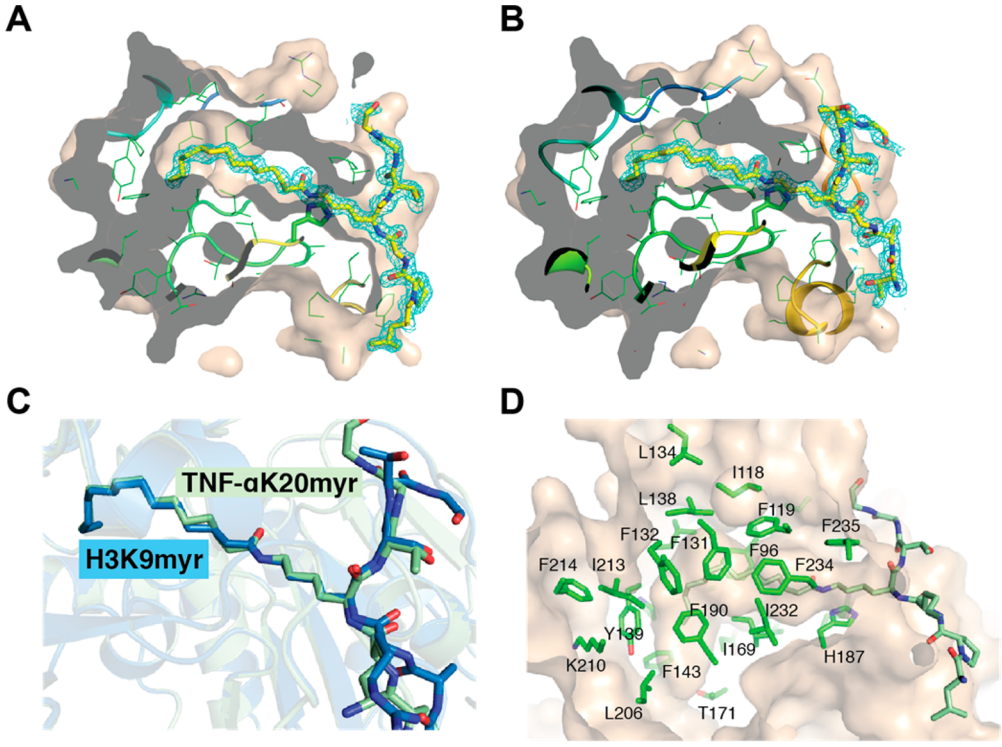

Figure 6. Analysis of the myristoyl-lysine-binding pocket. (A) $2F_o - F_c$ omit electron density map (cyan mesh, 1σ) of the TNF-αK20 myristoylated peptide. Molecular surfaces of SIRT2 cut at the level of the hydrophobic cavity are shown. The myristoylated peptides are drawn as sticks, in which yellow, blue, and red represent C, N, and O atoms, respectively. (B) $2F_o - F_c$ omit electron density map (cyan mesh, 1σ) of the H3K9 myristoylated peptide represented as shown in panel A. (C) Superimposition of SIRT2−TNFα-K20myr (light green) or SIRT2−H3K9myr (blue) highlighting the orientation of the myristoylated lysine chain. (D) Hydrophobic pocket in SIRT2 that accommodates the myristoyl chain.

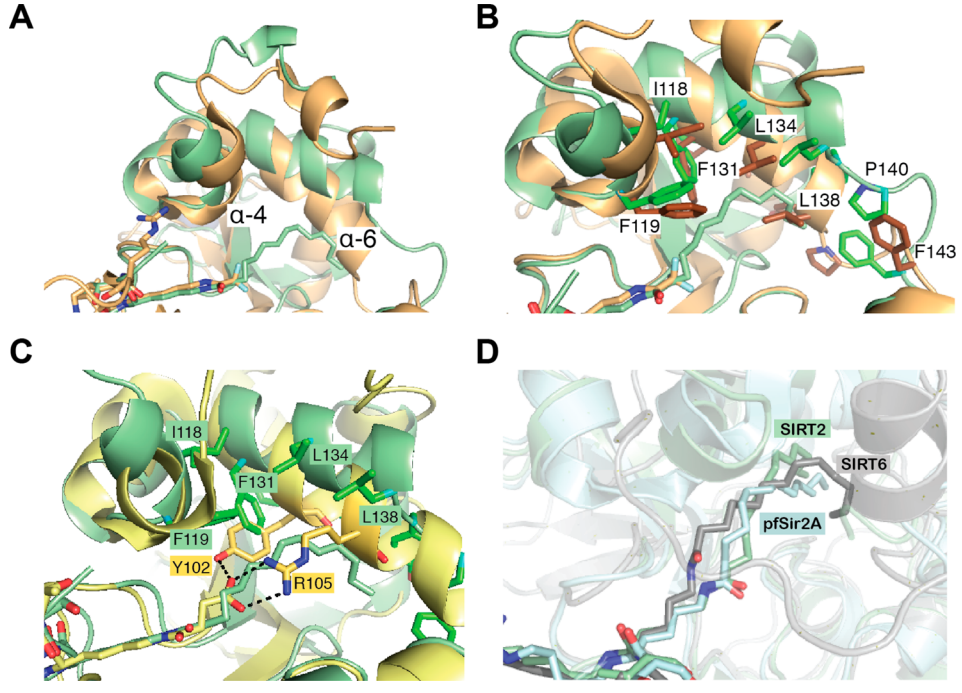

Figure 7. SIRT2−TNFα-K20myr structural comparison. (A) Superimposition of SIRT2−TNFα-K20myr (light green) with SIRT2−ε-trifluoroacetyl lysine peptide inhibitor (PDB entry 4L3O, brown), highlighting the differences in the helix bundle region. (B) Same structures as in panel A, highlighting the orientations of specific amino acids. (C) Superimposition of SIRT2−TNFα-K20myr (light green) with SIRT5−H3K9succinyl (PDB entry 4F4U, yellow). The amino acids in α-helix 6 that interact with the peptide substrates are shown as sticks. (D) Superimposition of SIRT2−TNFα-K20myr (light green) with SIRT6−H3K9myr (PDB entry 3ZG6, light blue) and pfSir2A−H3K9myr (PDB entry 3U3D, gray), highlighting the various orientations of the myristoyl group.

DOI: 10.1021/acs.biochem.5b00150
Biochemistry 2015, 54, 3037−3050

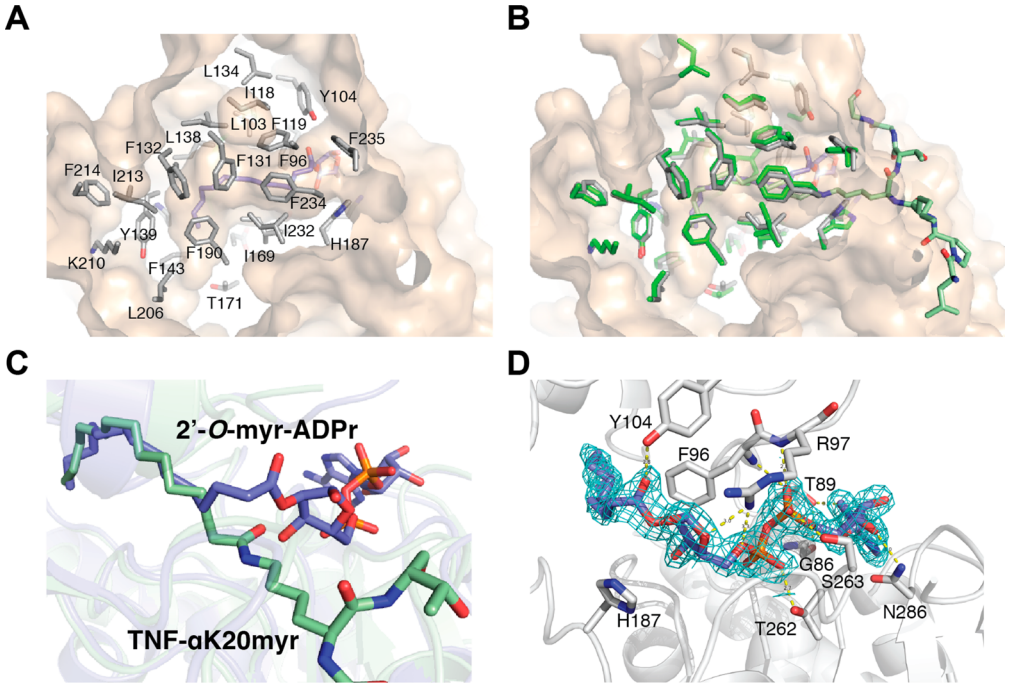

Figure 8. Comparison of SIRT2−2′-*O*-myristoyl-ADPr with SIRT2−TNFα-K20myr structure. (A) Hydrophobic pocket in SIRT2 that accommodates the myristoyl chain of 2′-*O*-myristoyl-ADPr. (B) Superimposition of SIRT2−2′-*O*-myristoyl-ADPr (gray) and SIRT2−TNFα-K20myr (green) structures highlighting the hydrophobic residues in the myristoyl chain-binding site. (C) Overlay as in panel B highlighting differences in the myristoyl chain between substrate and product. (D) $2F_o - F_c$ omit electron density map (blue mesh, 1σ) of the 2′-*O*-myristoyl-ADPr molecule and hydrogen bonding network surrounding 2′-*O*-myristoyl-ADPr. Also shown is the catalytic histidine residue.

concluded the myristoylated peptide should be in a trans conformation (Figure S4B of the Supporting Information). The newly refined structure was used in the comparison presented in Figure 7D.

Similar to the H3K9myr and TNF-αK20myr structures, the myristoyl chain of 2′-*O*-myristoyl-ADPr is bound in the hydrophobic pocket (Figure 8A), and there is minimal movement of the side chains (Figure 8B), indicating the hydrophobic pocket remains relatively unchanged during the course of the reaction. In support of this observation, superimposition of the TNF-αK20myr and 2′-*O*-myristoyl-ADPr structures reveals the majority of the myristoyl chain adopts a similar conformation between the substrate and product structures (Figure 8C) (rmsd of 1.2 Å). The difference between the acyl chains is found in C3, which is flipped and rotated in the myristoyl chain of 2′-*O*-myristoyl-ADPr. The movement is similar to what was previously observed in a cocrystal structure of SIRT5 in complex with the 1′,2′-cyclic intermediate. In the structure, the lysine side chain is rotated 18° and C3 of the succinyl group is flipped, while the carboxylate of the succinyl lysine remains in contact with Tyr-102 and Arg-105.[41] These observations suggest a general mechanism for facilitating deacylation of longer acyl substrates may be to hold the chain beyond C3 in a relatively fixed position during the reaction.

In addition to the rotation of C3 in 2′-*O*-myristoyl-ADPr, there is a corresponding rotation of C1′ and C2′ (Figure 8C) in the ribose. The orientation is stabilized by a hydrogen bond between the carbonyl oxygen and the hydroxyl group of Tyr-104 located in the cofactor-binding loop of SIRT2 (Figure 8D). The ADP-ribose interacts with SIRT2 through a number of side chain and backbone hydrogen bonds that are shown in Figure 8D. Interestingly, the catalytic histidine residue (His-187) does not hydrogen bond to the 3′-hydroxyl of the ribose as is observed in the SIRT5−cyclic intermediate structure (Figure 8D).[41]

DISCUSSION

The Kinetic Mechanism Demonstrates the Interdependence of NAD$^+$ Binding and Nicotinamide Inhibition on Specific Deacylation Reactions. We combined our NAD$^+$ steady-state kinetic, pre-steady-state, and inhibition analyses to develop a model for each Sirtuin that explains the relationship between NAD$^+$ binding and the acyl chain length of the peptide substrate. The established Sirtuin kinetic mechanism describes ordered binding of acyl-substrate followed by NAD$^+$ (Figure 1A).[24] Supraphysiological levels of NAD$^+$ can induce NAD$^+$ binding in nonproductive complexes in nonmammalian Sirtuins,[42,43] and near millimolar binding constants for NAD$^+$ for SIRT1 and SIRT3 have been measured *in vitro*.[44] However, to date only SIRT6 has been shown to bind NAD$^+$ tightly (K_D = 27 μM) in the absence of an acylated substrate,[22] suggesting SIRT6 may be capable of random substrate binding. In the case of random substrate binding to SIRT6, saturating with peptide will cause a random mechanism to behave as an ordered mechanism,[45] allowing us to utilize the same kinetic model to describe the behavior of all Sirtuins studied (Figure 1A).

The $k_{cat}/K_{m,NAD}$ values for SIRT1 are similar among all acyl-substrates analyzed (Figure 3). However, the k_{cat} value increased with the acetylated substrate compared to those with the longer acylated substrates (Figure 2A). The results suggest that as the acyl chain length increases, the rate of turnover is more adversely affected compared to the rate of NAD$^+$ capture by SIRT1 to form productive catalytic complexes. SIRT2, a cytosolic Sirtuin with protein substrates

DOI: 10.1021/acs.biochem.5b00150
Biochemistry 2015, 54, 3037−3050

distinct from those of SIRT1, displays trends in k_{cat} and $k_{cat}/K_{m,NAD}$ similar to those of SIRT1 (Figure 2A and 3). However, the catalytic efficiency is lower for SIRT2 in the presence of the longer acyl chains (Figure 3), indicating the decrease in $k_{cat}/K_{m,NAD}$ for SIRT2, particularly with the hexanoylated substrate, is driven by a weaker affinity of SIRT2 for NAD^+ or a decreased rate of NAD^+ cleavage (k_5) in the presence of the longer chain acyl groups compared to SIRT1 (Figure 3). The mitochondrial Sirtuin, SIRT3, displays trends different from those observed with SIRT1 and SIRT2. SIRT3 has the highest $k_{cat}/K_{m,NAD}$ for acetylated and myristoylated peptides (Figure 3) and the lowest for the hexanoylated substrate. The k_{cat} values are similar among the hexanoylated, deconylated, and myristoylated substrates (Figure 2A), while the K_m for NAD^+ is significantly higher in the presence of the hexanoylated substrate ($K_{m,NAD}$ of >910 μM for the hexanoylated substrate vs <75 μM for other substrates) (Figure 2B), indicating the rate of NAD^+ binding or cleavage is decreased. While use of the same peptide sequence for all Sirtuin isoforms allows for a dissection of the role of acyl chain length on catalysis, different amino acid sequences could impart additional kinetic differences.

The rate of partitioning of the C1′-*O*-alkylimidate intermediate between continuation to products and reversal to acylated substrate and NAD^+ dictates the sensitivity to nicotinamide inhibition, and the results indicate this partitioning is dependent on the acyl substrate. The slower conversion of the long chain *O*-alkylimidate intermediates (k_9) relative to deacetylation likely increases the sensitivity of SIRT2 to inhibition by nicotinamide, leading to decreases observed in nicotinamide IC_{50} with long chain acyl groups (Figure 4). Interestingly, nicotinamide is a more potent inhibitor of SIRT3 in the presence of the acetylated substrate. The result is similar to previous observations made for SIRT5,[44] a mitochondrial Sirtuin whose preferred desuccinylase activity is strongly inhibited by nicotinamide while the deacetylase activity displays very poor inhibition. Differences in nicotinamide inhibition with SIRT5 were proposed to be caused by differences in the organization of the active site in the presence of an acetylated peptide compared to a succinylated peptide.[44] Along with the data presented here, it is reasonable to suggest that the ability of nicotinamide to inhibit depends on the efficiency of binding the intermediate form of the enzyme, as well as the relative partitioning of the *O*-alkylimidate intermediates toward products or reactants.

To investigate in greater detail the individual steps in the SIRT2 and SIRT3 reactions that contribute to the observed patterns in the kinetic constants, pre-steady-state kinetics monitoring nicotinamide and deacylated peptide formation were performed with acetylated, hexanoylated, decanoylated, and myristoylated substrates. For all peptides analyzed, SIRT2 cleaved NAD^+ at a rate greater than k_{cat} (Table 1 and Figure 2A), which followed a similar trend to that observed for $k_{cat}/K_{m,NAD}$ (Figure 3 and Table 1). Therefore, nicotinamide formation (k_5) is not the rate-limiting step. The fold increases from hexanoylated to myristoylated substrates are similar to the changes in $k_{cat}/K_{m,NAD}$ (Figure 3 and Table S1 of the Supporting Information), indicating the increase in $k_{cat}/K_{m,NAD}$ is driven by a faster rate of NAD^+ cleavage (k_5), not a change in the rate of NAD^+ binding (k_3 and k_4) (Figure 1A). Similarly, SIRT3 cleaved NAD^+ at a rate greater than k_{cat} with all acylated substrates analyzed. However, as the chain length increases from acetyl to hexanoyl, the change in the rate of nicotinamide formation is significantly smaller than the fold change in $k_{cat}/K_{m,NAD}$ (Table S1 of the Supporting Information). Therefore, weaker binding of NAD^+ (k_3 and k_4) likely contributes to the decrease in $k_{cat}/K_{m,NAD}$ in the presence of the hexanoylated substrate as opposed to simply a decrease in the rate of NAD^+ cleavage (k_5).

A step after nicotinamide formation, either the second chemical step of the reaction (attack of 2′-OH on the imidate intermediate), hydrolysis of the cyclic intermediate, or product release (Figure 1A,B), is rate-limiting. Because the rapid-quench assay detects the formation of the deacylated product upon rapid quenching of the enzyme, the rate represents deacylated peptide formation of the labile 1′,2′-cyclic intermediate, which upon the acid quench yields deacylated product. Therefore, if all reaction steps prior to deacylated product and *O*-acyl-ADPr (*O*AADPr) release are faster than k_{cat}, we conclude that hydrolysis of the cyclic intermediate or the release of deacylated product or *O*AADPr must be rate-limiting. With acetylated, hexanoylated, decanoylated, and myristoylated substrates, SIRT2 and SIRT3 form deacylated peptide at rates similar to k_{cat} (≤2-fold) (Table 1 and Figure 2A), indicating the rate-limiting step of deacylation is the nucleophilic attack of the 2′-hydroxyl on the C1′-*O*-alkylimidate intermediate (k_9).

SIRT6, a Sirtuin with unique catalytic properties,[1] has a kinetic profile distinct from those of its paralogs, SIRT1–SIRT3. As acyl chain length increases, k_{cat} and k_{cat}/K_m increase (Figures 2A and 3). SIRT6 lacks the conserved helix bundle region, which we hypothesize is responsible for accommodating the acylated substrate in SIRT1–SIRT5 (Figure 7A,B). Instead, SIRT6 contains an extended N-terminal loop that covers the NAD^+- and acyl-substrate-binding sites.[2,22] Continuous electron density for the 12 N-terminal amino acids is observed only in the cocrystal structure of SIRT6 in complex with a myristoylated peptide and ADP-ribose, indicating the loop is highly flexible.[2] The ordering of the loop in the presence of the longer acyl chains might allow for synergistic binding of NAD^+ and secure the catalytically competent conformation, leading to an increased level of turnover (Figure 2A).

To determine whether the differing trend in k_{cat} from SIRT2 and SIRT3 could be explained by differences in the rate-limiting step of the reaction, we performed pre-steady-state kinetic analysis, and similar to those of SIRT2 and SIRT3, the rate of nicotinamide formation proceeds faster than k_{cat} with all peptides tested (Table 1 and Figure 2A). The increases in the rate of nicotinamide formation (k_5) are similar to the increases in $k_{cat}/K_{m,NAD}$ (Table 1, Table S1 of the Supporting Information, and Figure 3), indicating the increase in $k_{cat}/K_{m,NAD}$ is driven by faster NAD^+ cleavage (k_5) as opposed to differences in NAD^+ binding (k_3 and k_4).

We found that unlike SIRT2 and SIRT3, the rate-limiting step of the SIRT6 deacylation reaction appears to be dependent on acyl chain length. The rate of dehexanoyl product formation is equal to k_{cat}, while the rate of dodecanoyl and demyristoyl product formation is faster than k_{cat} (~3–4-fold) (Table 1 and Figure 2A). The results are consistent with the attack of the 2′-OH in the second chemical step (k_9) being rate-limiting in the dehexanoylation reaction, while hydrolysis of the 1′,2′-cyclic intermediate or the release of deacylated product or *O*AADPr appears to be the rate-limiting step with decanoylated and myristoylated substrates (Figure 1B). The rate of k_9 with the myristoylated substrate begins to approach the values observed for the more efficient SIRT2 and SIRT3 enzymes (Table 1), further highlighting the ability of SIRT6 to function as an efficient demyristoylase.

DOI: 10.1021/acs.biochem.5b00150
Biochemistry 2015, 54, 3037–3050

Taken together, the results indicate SIRT2 and SIRT3 may operate under the same kinetic mechanism where the same rate-limiting step is maintained among the diverse acyl substrates, while the nature of the rate-limiting step of SIRT6 depends on the length of the acyl chain. With the exception of SIRT2 and SIRT3 with the myristoylated substrate, while the individual rates of k_5 and k_9 differ between Sirtuins and between peptides, the difference between the rates of k_5 and k_9 for a given Sirtuin and substrate are within an order of magnitude of each other (Table 1). This suggests the rate of NAD^+ cleavage is coupled to the rate of attack of the 2′-hydroxyl on the C1′-*O*-alkylimidate intermediate, such that the rate of NAD^+ cleavage does not far exceed the rate of the second chemical step.

Structural Insight into Long Chain Deacylation. Long chain deacylation was initially believed to be limited to SIRT6 and pfSir2A, because of the identification of a hydrophobic binding cavity for the longer acyl groups. However, our previous[1] and current analyses demonstrate human Sirtuins SIRT1−SIRT3 function as efficient long chain deacylases. The crystal structures of SIRT2-bound myristoylated substrates identified a latent hydrophobic binding pocket, which is able to accommodate the longer myristoyl chain (Figure 6D). SIRT1 and SIRT3 have similarly positioned hydrophobic amino acids (Figure S5 of the Supporting Information), indicating these Sirtuins have a latent hydrophobic binding pocket to accommodate the long acyl chains, as evidenced by long chain deacylation activity. Additionally, structural alignment of SIRT2 in complex with a myristoyl-lysine peptide or an ε-trifluoroacetyl-lysine peptide identified α-helices 4 and 6 in the helix bundle region as having the largest conformational change in the presence of the myristoyl chain compared to the smaller ε-trifluoroacetyl ligand (Figure 7A). The movement places several hydrophobic amino acids in a position to bind the myristoyl chain. The amino acids are similar in SIRT1 and SIRT3; however, Phe-312 and Ile-316 in SIRT1 are larger than the respective leucine residues in SIRT2 and SIRT3 (Figure S5 of the Supporting Information). The increased van der Waals forces and size of the amino acids might help lock the longer acyl chains and NAD^+ in a suitable conformation for catalysis, leading to the observed increase in $k_{cat}/K_{m,NAD}$ with the longer acyl chains. Despite having very similar hydrophobic pockets, SIRT2 and SIRT3 display varying catalytic efficiencies that depend on the nature of the acylated substrate, indicating there are additional factors that affect NAD^+ capture ($k_{cat}/K_{m,NAD}$) that would not be evident from the crystal structure alone. These differences include the dynamics of the acyl-substrate-binding pocket for each Sirtuin as well as the highly flexible cofactor-binding loop,[39] which adopts different conformations depending on the ligand(s) bound. However, the k_9 rates for SIRT2 and SIRT3 are similar among the hexanoylated, decanoylated, and myristoylated intermediates (Table S1 of the Supporting Information), suggesting once the *O*-alkylimidate intermediate is formed, the chain is held in a similar conformation allowing for attack of 2′-hydroxyl (Figure 1B).

***In Vivo* Implications.** Genetically, metabolically, and pharmacologically induced alterations in NAD^+ levels have been linked to changes in Sirtuin activity.[17] However, inconsistent observations have confounded a clear picture of the connection between NAD^+ and each Sirtuin. Here, we provide a model that describes the interrelationships among the different deacylation specificities, the NAD^+ dependence, and the chemical mechanism of individual human Sirtuin members. These results have broad implications and provide molecular insight into the cellular behavior of Sirtuin activity. NAD^+ is an essential cosubstrate in metabolism, and its biosynthesis is compartmentalized.[46] Studies estimate cellular levels of NAD^+ to be 365 μM with 70% of this pool located in the mitochondria and 10−100 μM in the nucleus and cytoplasm.[8,47] Consistent with adaptation to compartmentalized NAD^+, mitochondrial SIRT3 has a K_m for NAD^+ with all substrates tested higher than those for the nuclear and cytoplasmic Sirtuins (Figure 2B).

Taken together, our observations support the idea that individual Sirtuin activity has evolved to operate in a subcellular compartment where changes in NAD^+ levels will directly affect Sirtuin activity and substrate preference. Moreover, the generally low K_m values for NAD^+ with long chain acyl substrates combined with the low K_m values for long chain acyl substrates suggest that these deacylations are not controlled appreciably by cellular NAD^+ fluctuations and might reflect a housekeeping function to limit the adverse effects of spurious long chain protein acylation from acyl-CoAs. The low K_m values are indicative of a strong commitment to catalysis when Sirtuins encounter these modifications in the cell. Recent literature suggests many acyl-lysine modifications exist *in vivo*, and much remains to be explored about the potential Sirtuin substrates that contain these modifications.[2,3,9,13−16]

CONCLUDING REMARKS

We present an integrated kinetic and structural analysis providing insight into potential regulation of *in vivo* Sirtuin activity. We find the K_m for NAD^+ and susceptibility to nicotinamide inhibition vary with Sirtuin and are dependent upon the acyl substrate. Nicotinamide is considered a general Sirtuin product inhibitor and widely used in studies *in vivo* and *in vitro*. Our results reveal careful consideration should be taken when using this commonly employed Sirtuin inhibitor in cell-based and *in vitro* studies and suggest targeted nicotinamide inhibition is possible. We provide the first rapid-quench analysis of human Sirtuins, showing nicotinamide formation is rapid when compared to product formation or release for SIRT2, SIRT3, and SIRT6 for all acylated substrates tested. Rapid-quench analysis establishes that the nucleophilic attack of the 2′-hydroxyl on the C1′-*O*-alkylimidate intermediate is the rate-limiting step of catalysis for SIRT2 and SIRT3 and is independent of the acylated substrate, while the rate-limiting step for SIRT6 depends on the length of the acyl chain and appears to change from attack of the 2′-hydroxyl group with the hexanoylated substrate to the hydrolysis of the cyclic intermediate or the release of deacylated product or *O*AADPr with decanoylated or myristoylated substrates. Our structural studies indicate the myristoyl chain is held in a relatively fixed position during catalysis and reveals a general mechanism for long chain deacylation. Taken together, this study establishes the interdependence of NAD^+ binding, acyl-substrate, and nicotinamide inhibition on the Sirtuin chemical mechanism. As diverse deacylation activities for Sirtuins are further characterized in cells, this compilation of kinetic parameters will support the development of targeted small molecule inhibitors and activators.

ASSOCIATED CONTENT

Supporting Information

NAD^+ saturation curves (Figure S1), nicotinamide inhibition curves (Figure S2), single-turnover kinetics (Figure S3),

DOI: 10.1021/acs.biochem.5b00150
Biochemistry 2015, 54, 3037−3050

rerefinement of the SIRT6 coordinates in complex with a myristoylated peptide (Figure S4), a sequence alignment (Figure S5), and rate constant comparisons (Table S1). The Supporting Information is available free of charge on the ACS Publications website at DOI: 10.1021/acs.biochem.5b00150.

AUTHOR INFORMATION

Corresponding Authors

*E-mail: jmdenu@wisc.edu.
*E-mail: yoshidam@riken.jp.

Present Address

[@]K.E.D.-R.: Laboratory of Systems Biology, Van Andel Research Institute, Grand Rapids, MI 49503.

Author Contributions

J.L.F., K.E.D.-R., and N.K. contributed equally to this work.

Funding

This work was supported by National Institutes of Health (NIH) Traineeship 5T32GM08349 (K.E.D.-R.), NIH Grant GM06538 (J.M.D.), and the Project for Development of Innovative Research on Cancer Therapeutics (P-DIRECT) from The Ministry of Education, Culture, Sports, Science and Technology of Japan (A.I.). The purchase of the Bruker REFLEXII instrument in 1996 was partially funded by National Science Foundation Award 9520868 to the University of Wisconsin—Madison Department of Chemistry.

Notes

The authors declare no competing financial interest.

ABBREVIATIONS

NAD^+, nicotinamide adenine dinucleotide; NAM, nicotinamide; TNFα, tumor necrosis factor α; *O*AADPR, *O*-acyl-ADP-ribose; Myr, myristoyl; DMF, dimethylformamide; DCM, dichloromethane; TFA, trifluoroacetic acid.

REFERENCES

(1) Feldman, J. L., Baeza, J., and Denu, J. M. (2013) Activation of the protein deacetylase SIRT6 by long-chain fatty acids and widespread deacylation by mammalian sirtuins. *J. Biol. Chem. 288*, 31350−31356.

(2) Jiang, H., Khan, S., Wang, Y., Charron, G., He, B., Sebastian, C., Du, J., Kim, R., Ge, E., Mostoslavsky, R., Hang, H. C., Hao, Q., and Lin, H. (2013) SIRT6 regulates TNF-α secretion through hydrolysis of long-chain fatty acyl lysine. *Nature 496*, 110−113.

(3) Wagner, G. R., and Hirschey, M. D. (2014) Nonenzymatic protein acylation as a carbon stress regulated by sirtuin deacylases. *Mol. Cell 54*, 5−16.

(4) He, W., Newman, J. C., Wang, M. Z., Ho, L., and Verdin, E. (2012) Mitochondrial sirtuins: Regulators of protein acylation and metabolism. *Trends Endocrinol. Metab. 23*, 467−476.

(5) Cai, L., Sutter, B. M., Li, B., and Tu, B. P. (2011) Acetyl-CoA induces cell growth and proliferation by promoting the acetylation of histones at growth genes. *Mol. Cell 42*, 426−437.

(6) Weinert, B. T., Iesmantavicius, V., Moustafa, T., Scholz, C., Wagner, S. A., Magnes, C., Zechner, R., and Choudhary, C. (2014) Acetylation dynamics and stoichiometry in *Saccharomyces cerevisiae*. *Mol. Syst. Biol. 10*, 716.

(7) Weinert, B. T., Iesmantavicius, V., Wagner, S. A., Scholz, C., Gummesson, B., Beli, P., Nystrom, T., and Choudhary, C. (2013) Acetyl-phosphate is a critical determinant of lysine acetylation in *E. coli*. *Mol. Cell 51*, 265−272.

(8) Lombard, D. B., Alt, F. W., Cheng, H. L., Bunkenborg, J., Streeper, R. S., Mostoslavsky, R., Kim, J., Yancopoulos, G., Valenzuela, D., Murphy, A., Yang, Y., Chen, Y., Hirschey, M. D., Bronson, R. T., Haigis, M., Guarente, L. P., Farese, R. V., Jr., Weissman, S., Verdin, E., and Schwer, B. (2007) Mammalian Sir2 homolog SIRT3 regulates global mitochondrial lysine acetylation. *Mol. Cell. Biol. 27*, 8807−8814.

(9) Du, J., Zhou, Y., Su, X., Yu, J. J., Khan, S., Jiang, H., Kim, J., Woo, J., Kim, J. H., Choi, B. H., He, B., Chen, W., Zhang, S., Cerione, R. A., Auwerx, J., Hao, Q., and Lin, H. (2011) Sirt5 is a NAD-dependent protein lysine demalonylase and desuccinylase. *Science 334*, 806−809.

(10) Garrity, J., Gardner, J. G., Hawse, W., Wolberger, C., and Escalante-Semerena, J. C. (2007) N-Lysine propionylation controls the activity of propionyl-CoA synthetase. *J. Biol. Chem. 282*, 30239−30245.

(11) Liu, B., Lin, Y., Darwanto, A., Song, X., Xu, G., and Zhang, K. (2009) Identification and characterization of propionylation at histone H3 lysine 23 in mammalian cells. *J. Biol. Chem. 284*, 32288−32295.

(12) Zhang, K., Chen, Y., Zhang, Z., and Zhao, Y. (2009) Identification and verification of lysine propionylation and butyrylation in yeast core histones using PTMap software. *J. Proteome Res. 8*, 900−906.

(13) Zhang, Z., Tan, M., Xie, Z., Dai, L., Chen, Y., and Zhao, Y. (2011) Identification of lysine succinylation as a new post-translational modification. *Nat. Chem. Biol. 7*, 58−63.

(14) Peng, C., Lu, Z., Xie, Z., Cheng, Z., Chen, Y., Tan, M., Luo, H., Zhang, Y., He, W., Yang, K., Zwaans, B. M., Tishkoff, D., Ho, L., Lombard, D., He, T. C., Dai, J., Verdin, E., Ye, Y., and Zhao, Y. (2011) The first identification of lysine malonylation substrates and its regulatory enzyme. *Mol. Cell. Proteomics 10*, M111 012658.

(15) Xie, Z., Dai, J., Dai, L., Tan, M., Cheng, Z., Wu, Y., Boeke, J. D., and Zhao, Y. (2012) Lysine succinylation and lysine malonylation in histones. *Mol. Cell. Proteomics 11*, 100−107.

(16) Tan, M., Peng, C., Anderson, K. A., Chhoy, P., Xie, Z., Dai, L., Park, J., Chen, Y., Huang, H., Zhang, Y., Ro, J., Wagner, G. R., Green, M. F., Madsen, A. S., Schmiesing, J., Peterson, B. S., Xu, G., Ilkayeva, O. R., Muehlbauer, M. J., Braulke, T., Muhlhausen, C., Backos, D. S., Olsen, C. A., McGuire, P. J., Pletcher, S. D., Lombard, D. B., Hirschey, M. D., and Zhao, Y. (2014) Lysine glutarylation is a protein posttranslational modification regulated by SIRT5. *Cell Metab. 19*, 605−617.

(17) Imai, S. I., and Guarente, L. (2014) NAD and sirtuins in aging and disease. *Trends Cell Biol. 24*, 464−471.

(18) Frye, R. A. (2000) Phylogenetic classification of prokaryotic and eukaryotic Sir2-like proteins. *Biochem. Biophys. Res. Commun. 273*, 793−798.

(19) Borra, M. T., Smith, B. C., and Denu, J. M. (2005) Mechanism of human SIRT1 activation by resveratrol. *J. Biol. Chem. 280*, 17187−17195.

(20) Borra, M. T., O'Neill, F. J., Jackson, M. D., Marshall, B., Verdin, E., Foltz, K. R., and Denu, J. M. (2002) Conserved enzymatic production and biological effect of O-acetyl-ADP-ribose by silent information regulator 2-like NAD^+-dependent deacetylases. *J. Biol. Chem. 277*, 12632−12641.

(21) Hallows, W. C., Lee, S., and Denu, J. M. (2006) Sirtuins deacetylate and activate mammalian acetyl-CoA synthetases. *Proc. Natl. Acad. Sci. U.S.A. 103*, 10230−10235.

(22) Pan, P. W., Feldman, J. L., Devries, M. K., Dong, A., Edwards, A. M., and Denu, J. M. (2011) Structure and biochemical functions of SIRT6. *J. Biol. Chem. 286*, 14575−14587.

(23) Cleland, W. W. (1975) Partition analysis and the concept of net rate constants as tools in enzyme kinetics. *Biochemistry 14*, 3220−3224.

(24) Borra, M. T., Langer, M. R., Slama, J. T., and Denu, J. M. (2004) Substrate specificity and kinetic mechanism of the Sir2 family of NAD^+-dependent histone/protein deacetylases. *Biochemistry 43*, 9877−9887.

(25) Northrop, D. B. (1998) On the Meaning of K_m and V/K in Enzyme Kinetics. *J. Chem. Educ. 75*, 1153.

(26) Smith, B. C., and Denu, J. M. (2007) Sir2 deacetylases exhibit nucleophilic participation of acetyl-lysine in NAD^+ cleavage. *J. Am. Chem. Soc. 129*, 5802−5803.

(27) Wu, J., Xie, N., Wu, Z., Zhang, Y., and Zheng, Y. G. (2009) Bisubstrate Inhibitors of the MYST HATs Esa1 and Tip60. *Bioorg. Med. Chem. 17*, 1381−1386.

DOI: 10.1021/acs.biochem.5b00150
Biochemistry 2015, 54, 3037−3050

(28) Otwinowski, Z., and Minor, W. (1997) Processing of X-ray diffraction data collected in oscillation mode. *Methods Enzymol. 276*, 307−326.
(29) Winn, M. D., Ballard, C. C., Cowtan, K. D., Dodson, E. J., Emsley, P., Evans, P. R., Keegan, R. M., Krissinel, E. B., Leslie, A. G., McCoy, A., McNicholas, S. J., Murshudov, G. N., Pannu, N. S., Potterton, E. A., Powell, H. R., Read, R. J., Vagin, A., and Wilson, K. S. (2011) Overview of the CCP4 suite and current developments. *Acta Crystallogr. D67*, 235−242.
(30) Murshudov, G. N., Vagin, A. A., and Dodson, E. J. (1997) Refinement of macromolecular structures by the maximum-likelihood method. *Acta Crystallogr. D53*, 240−255.
(31) Emsley, P., Lohkamp, B., Scott, W. G., and Cowtan, K. (2010) Features and development of Coot. *Acta Crystallogr. D66*, 486−501.
(32) Chen, V. B., Arendall, W. B., III, Headd, J. J., Keedy, D. A., Immormino, R. M., Kapral, G. J., Murray, L. W., Richardson, J. S., and Richardson, D. C. (2010) MolProbity: All-atom structure validation for macromolecular crystallography. *Acta Crystallogr. D66*, 12−21.
(33) Jackson, M. D., Schmidt, M. T., Oppenheimer, N. J., and Denu, J. M. (2003) Mechanism of nicotinamide inhibition and transglycosidation by Sir2 histone/protein deacetylases. *J. Biol. Chem. 278*, 50985−50998.
(34) Smith, B. C., and Denu, J. M. (2007) Sir2 deacetylases exhibit nucleophilic participation of acetyl-lysine in NAD^+ cleavage. *J. Am. Chem. Soc. 129*, 5802−5803.
(35) Yamagata, K., Goto, Y., Nishimasu, H., Morimoto, J., Ishitani, R., Dohmae, N., Takeda, N., Nagai, R., Komuro, I., Suga, H., and Nureki, O. (2014) Structural basis for potent inhibition of SIRT2 deacetylase by a macrocyclic peptide inducing dynamic structural change. *Structure 22*, 345−352.
(36) Moniot, S., Schutkowski, M., and Steegborn, C. (2013) Crystal structure analysis of human Sirt2 and its ADP-ribose complex. *J. Struct. Biol. 182*, 136−143.
(37) Finnin, M. S., Donigian, J. R., and Pavletich, N. P. (2001) Structure of the histone deacetylase SIRT2. *Nat. Struct. Biol. 8*, 621−625.
(38) Teng, Y. B., Jing, H., Aramsangtienchai, P., He, B., Khan, S., Hu, J., Lin, H., and Hao, Q. (2015) Efficient Demyristoylase Activity of SIRT2 Revealed by Kinetic and Structural Studies. *Sci. Rep. 5*, 8529.
(39) Sanders, B. D., Jackson, B., and Marmorstein, R. (2010) Structural basis for sirtuin function: What we know and what we don't. *Biochim. Biophys. Acta 1804*, 1604−1616.
(40) Zhu, A. Y., Zhou, Y., Khan, S., Deitsch, K. W., Hao, Q., and Lin, H. (2012) *Plasmodium falciparum* Sir2A preferentially hydrolyzes medium and long chain fatty acyl lysine. *ACS Chem. Biol. 7*, 155−159.
(41) Zhou, Y., Zhang, H., He, B., Du, J., Lin, H., Cerione, R. A., and Hao, Q. (2012) The bicyclic intermediate structure provides insights into the desuccinylation mechanism of human sirtuin 5 (SIRT5). *J. Biol. Chem. 287*, 28307−28314.
(42) Avalos, J. L., Boeke, J. D., and Wolberger, C. (2004) Structural basis for the mechanism and regulation of Sir2 enzymes. *Mol. Cell 13*, 639−648.
(43) Min, J., Landry, J., Sternglanz, R., and Xu, R. M. (2001) Crystal structure of a SIR2 homolog-NAD complex. *Cell 105*, 269−279.
(44) Fischer, F., Gertz, M., Suenkel, B., Lakshminarasimhan, M., Schutkowski, M., and Steegborn, C. (2012) Sirt5 deacylation activities show differential sensitivities to nicotinamide inhibition. *PLoS One 7*, e45098.
(45) Cook, P. F., and Cleland, W. W. (2007) *Enzyme kinetics and mechanism*, Garland Science, London.
(46) Nikiforov, A., Dolle, C., Niere, M., and Ziegler, M. (2011) Pathways and subcellular compartmentation of NAD biosynthesis in human cells: From entry of extracellular precursors to mitochondrial NAD generation. *J. Biol. Chem. 286*, 21767−21778.
(47) Zhang, Q., Piston, D. W., and Goodman, R. H. (2002) Regulation of corepressor function by nuclear NADH. *Science 295*, 1895−1897.

DOI: 10.1021/acs.biochem.5b00150
Biochemistry 2015, 54, 3037−3050